J. Inst. Eng. India Ser. C (January–March 2013) 94(1):85–91
DOI 10.1007/s40032-012-0052-y

CASE STUDY

Numerical Prediction of Surface Heat Flux During Multiple Jets Firing for Missile Control

S. Saha · P. K. Sinha · D. Chakraborty

Received: 9 December 2011 / Accepted: 21 November 2012 / Published online: 20 March 2013

Abstract Numerical simulations are carried out to obtain the flowfield and heat flux arising out of the flow interactions of different control thrusters viz. vernier, pitch, yaw, roll and divert thruster among themselves as well as with free stream at different altitudes of operation. Three critical points on a typical trajectory of a missile are chosen and combinations of the thrusters operating at those conditions are considered. Simulations have also been performed to simulate DT motor interaction with free stream at different altitude. The interaction of different motor flowfield with the free stream presents a very complex flowfield. Flow gradients are very high close to the nozzle exit because of high altitude operation of motors. 3-Dimensional RANS equations are solved along with k-ε turbulence model on unstructured tetrahedral grid using commercial CFD software. The flow properties along with the surface heat flux distribution for four isothermal wall temperatures 350, 450, 550, 650 K are computed and provided for surface temperature prediction. It is observed that with increase in altitude, the high heat flux region reduces and heat transfer coefficient is independent of wall temperature.

Keyword CFD · Heat flux · Missile control · Reaction control system

Introduction

The control demand for higher agility and enhanced maneuverability of a missile can be realised by side jet control. Although, the aerodynamic control surfaces work more efficiently in high densities and high velocities, the side jet control has quick response time compared to the aerodynamic control and works in low stagnation pressure in the launch phase or low pressure at high altitude [1, 2]. In its passive state, side jet control produces no additional drag as none of its components intrudes in the flow path. Thus lateral jet attitude control has been a preferred concept for missile systems.

Champigny and Lacau [1] presented a detailed review of transverse jet exhausted into supersonic free stream. The interaction of the jet with the free stream, produce a complex flow structure consisting of a bow shock, separation region ahead of the jet, barrel shock and counter rotating vortex pair in the wake of the jet. Controlling the overpressure ahead of the side jet and the under pressure downstream regions by suitable location and operation of jets, the desired control forces can be achieved. The flow structure of transverse jet in supersonic cross stream is shown schematically by Ben-Yakar et al. [2] and is reproduced in Fig. 1. The operating altitude, free stream Mach number, pressure ratios of the jet and free stream, diameter and shape of the side jet nozzle etc. have significant effect on the jet shape and its penetration into the supersonic free stream. Recent advances of CFD have enabled direct solution of jet interaction flowfield under many circumstances of application interest. Cassel [3] brought out the effect of various aerodynamic interference problems on experimental and analytical modeling of jet interaction technology for aerospace vehicle control and proposed a combination of CFD, wind tunnel and flight testing to understand the complex flow characteristics of jet interaction problem. The status of present CFD studies in the jet interaction problem is available in Ref. [4]. Aswin and Chakraborty [4] have carried out systematic

S. Saha · P. K. Sinha (✉) · D. Chakraborty
CCD Division, DOCD, Defence Research and Development Laboratory, Hyderabad 500 058, India
e-mail: pksinha@drdl.drdo.in

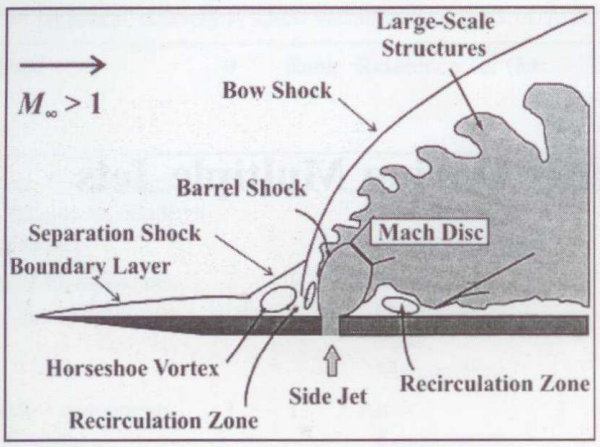

Fig. 1 Schematic of transverse jet injection flow field (from Ref. [2])

comparison of numerical experimental data for different angle of attack, ratios of free stream and jet pressure, number of jets, etc.

While using the lateral jet control, special attention need to be given to the thermal safety of the airframe. As the hot jet from motors interact with the freestream, the hot gas gazed over the missile surface. Recirculating flow ahead of the jet and the low pressure region downstream of jet also aid the hot motor exhaust passes through the missile body. When pitch, roll and yaw controls are required together, number of hot jets are employed and the situation becomes more complicated. The motor plumes interact with each other as well as with the free stream and create a complex flow pattern around the missile body. For proper design of airframe thermal protection system, study of this complex flowfield is very much necessary and CFD tools are used to assess the thermal environment as well as for estimation of heat flux, required for thermo-structural analysis. In this study, numerical simulations are carried out for the prediction of thermal environment i.e. gas temperature and heat flux on the missile surface during firing of multiple hot jets (RCS). 3-Dimensional (3-D) Navier–Stokes Equations along with k-ε turbulence model have been solved using commercial software CFX-10 [5]. The effect of altitude on the surface heat flux also has been brought out for single motor [divert thruster (DT)] firing. The methodology is validated [4] by comparing the numerical results with experimental results of transverse multiple jet in supersonic free stream. Both adiabatic and isothermal wall conditions are simulated for different wall temperatures (350, 450, 550 and 650 K) and for different combination of control thruster firing. The computed flow parameters and heat flux data have formed a valuable input for thermo structural analysis of missile airframe.

Geometry and Grid Generations

The geometry of the missile airframe with various RCS motors and the Divert Thruster (DI) is shown in Fig. 2a and b. The roll, pitch and yaw motors are located in the same axial plane ahead of the base. There are two vernier motors (vernier 1 and 2) and one DT motor in the same axial location in the middle of the missile. Three critical cases, from the jet interaction point of view, are identified from missile trajectory where only a specific set of motors are fired simultaneously and simulations are performed for those conditions.

Three dimensional unstructured tetrahedral grids are generated using CFX-Build 5.6 [6] around the missile and inside the motor nozzles. Extruded prism cells have been generated near the walls to capture the sharp gradients in the boundary layer. The outer domain for all the simulations have been chosen in such a way that the shock formed in front of the jet does not hit the inlet boundary. Typical

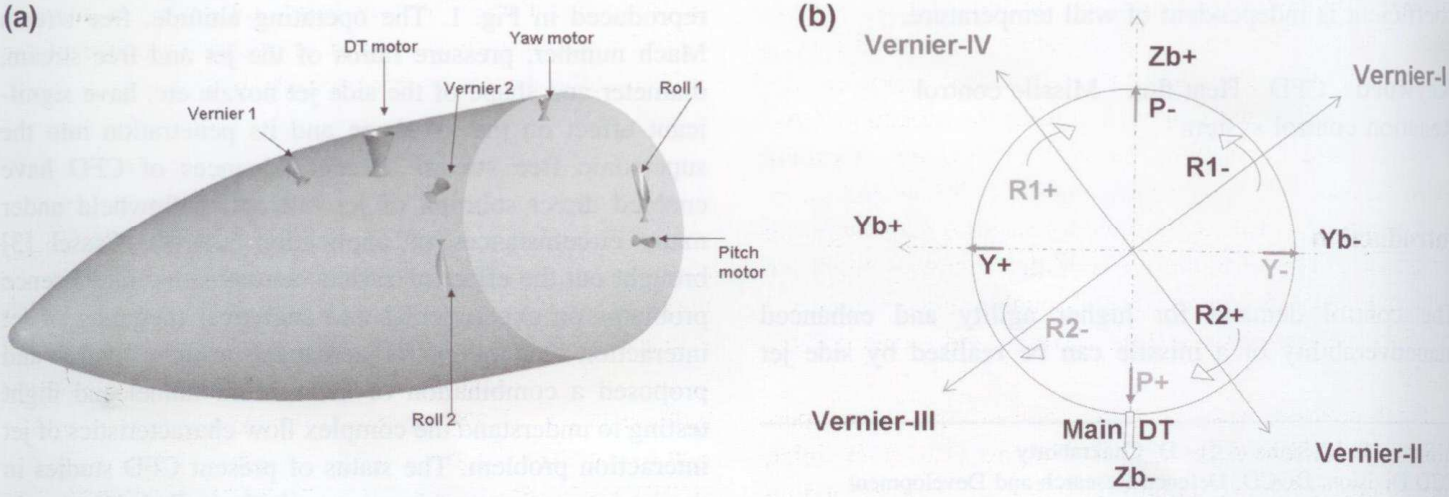

Fig. 2 **a** Geometry showing the motors. **b** Relative circumferential placement of motors

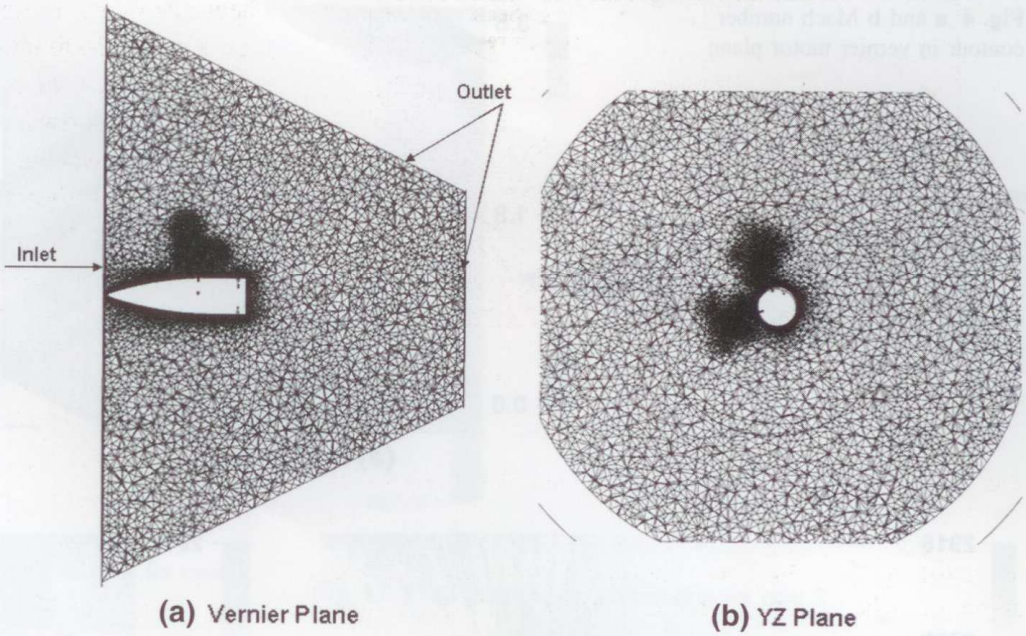

Fig. 3 Unstructured tetrahedral grid around vernier motors. **a** Vernier plane, **b** YZ plane

unstructured grid distribution in a plane passing through one of the vernier motor and a cross-sectional plane through vernier motors are shown in Fig. 3a and b respectively. The operation altitude (above 45 km) being very high, the jet pressure ratios (for vernier motor) are also very high ($P_e/P_\infty \sim 2{,}000$) creating a very high gradient around jets. Hence, sufficient clustering of the grid has been done around the motor region to capture the flow properties accurately. Typical grid size is about 3 million cells with minimum y^+ ($\sim$) 50.

Solution Methodology

Commercial CFD software, CFX 10 [5] is used for the simulation. This software solves 3-D Reynolds averaged Navier–Stokes (RANS) equation based on finite volume approach. It has following turbulence models viz. k-ε, k-ω or SST turbulence model, etc. for closure of RANS equations. The parallel version of the software is used for the simulation. The software has four major modules viz. (a) *CFX Build*, used for importing or creating CAD geometry and generating unstructured volume meshing based on the user input (b) boundary conditions and initial field condition are set up in the *preprocessor* (c) solution of the flowfield based on the grid and the boundary condition is initiated and monitored through *solver manager* (d) *postprocessor* is used to extract and visualize the results.

Total pressure and total temperature conditions pertaining to different motors are imposed at their inlet. Supersonic boundary condition with the corresponding velocities, free stream pressure and angle of attack is imposed at the free stream inlet. Supersonic outflow boundary condition is prescribed at the outlet. No-slip boundary condition for velocity and adiabatic condition for temperature are imposed on all the solid walls in case of adiabatic simulations and a fixed wall temperatures of 450 and 350 K are used for isothermal simulations. For the simulations k-ε turbulence model and first order upwind scheme for inviscid flux are used. Two species namely air and combustion gas has been solved. RMS residual level of 1e-5 of mass, momentum, energy and turbulence equations is kept as convergence criteria.

Flow Conditions

The RCS motor operating altitude, Mach No. and angle of attack are in the range of 45–52.5 km, 2.35–2.6 and 0–5° respectively. Three different cases are simulated numerically by varying altitudes and the firing sequence of the RCS motors. The cases corresponds to

Table 1 Chamber conditions of the motors

Parameters	DT motor	Vernier motor	Pitch motor	Yaw motor	Roll motor
$\dot{m}$ (kg/s)	5.656	0.9343	0.28	0.28	0.0773
P_0 (bar)	55	23.59	23.11	23.11	23.11
T_0 (K)	3,658	2,936	2,936	2,936	2,936
P_e/P_∞ at 45 km	728	660	245	245	17
P_e/P_∞ at 52.5 km	1,896	1,724	638	638	43

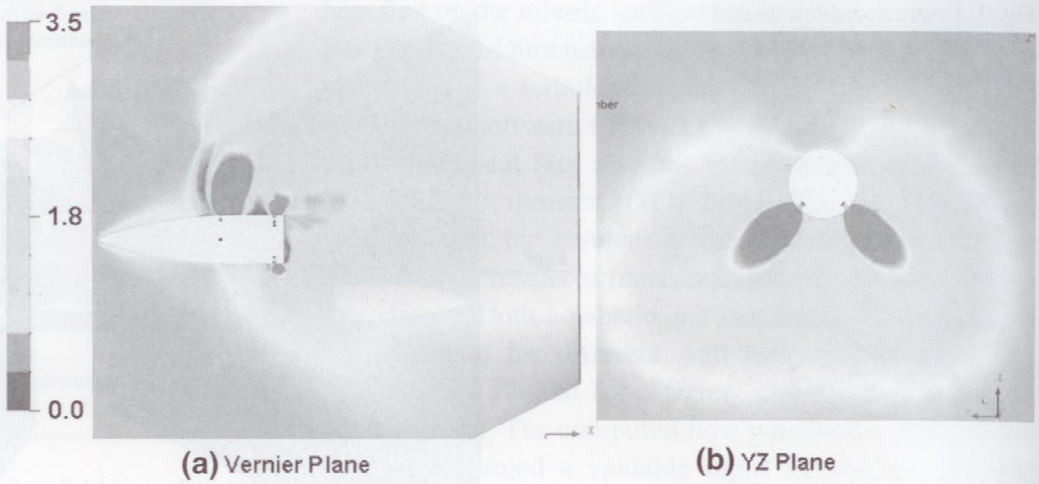

Fig. 4 **a** and **b** Mach number contour in vernier motor plane

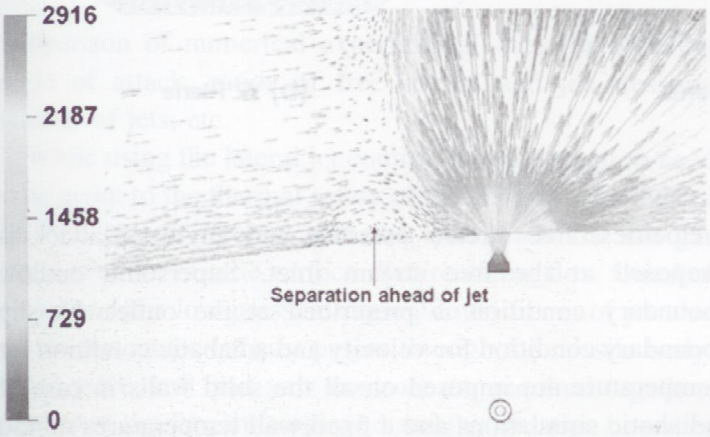

Fig. 5 Zoomed view of vector plot showing recirculation ahead of vernier jet

(1) Firing of two vernier motors, two roll motors and one yaw motor at 45 km altitude.
(2) Firing of two vernier motors, two roll motors, one yaw motor and one pitch motor at 52.5 km altitude.
(3) Firing of DT at 45 and 52.5 km.

The mass flow rate and chamber conditions for various RCS, vernier and DT motor are tabulated in Table 1.

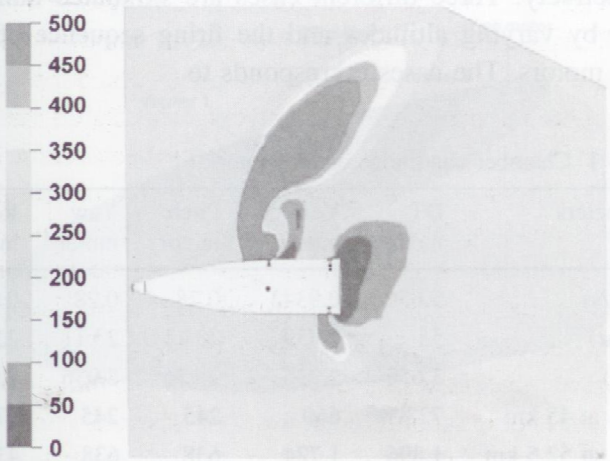

Fig. 6 Static pressure contour in vernier motor plane

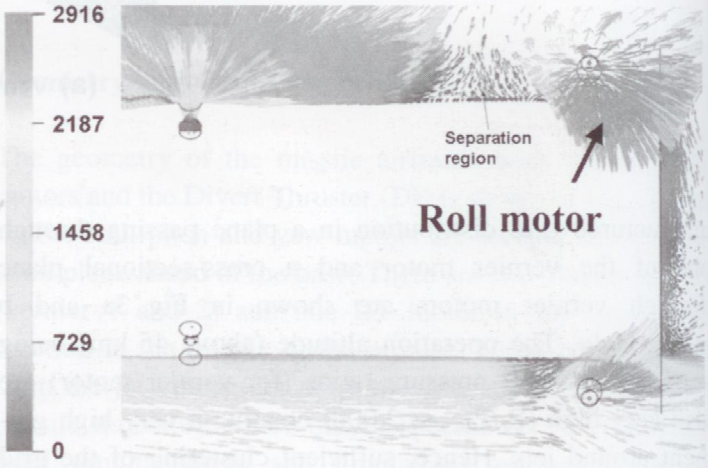

Fig. 7 Velocity vector showing separation ahead of roll motor plume

Results and Discussions

Case 1: Interaction of Vernier, Yaw and Roll Control Motor at 45 km

The simulation pertains to firing of two vernier motors (II and III), two roll motors (R1− and R2−) and one yaw motor (Y+) with a free stream pressure and temperature of 151 Pa and 265 K respectively. The Mach number contour in a plane passing through one of the vernier motors and in cross-sectional plane passing through the vernier motors are plotted in Fig. 4a and b respectively. Though the roll motors are placed at a different circumferential location with respect to vernier motor, their effect is seen in Mach number contour in Fig. 4a because of their inclined jet direction. The flow features characteristic of a cross flow injection in a supersonic stream can be seen in Fig. 4a, especially the bow shock in front of the expanding plume and the flow separation ahead of the jet. The three dimensional expansion of the jets and the interaction of

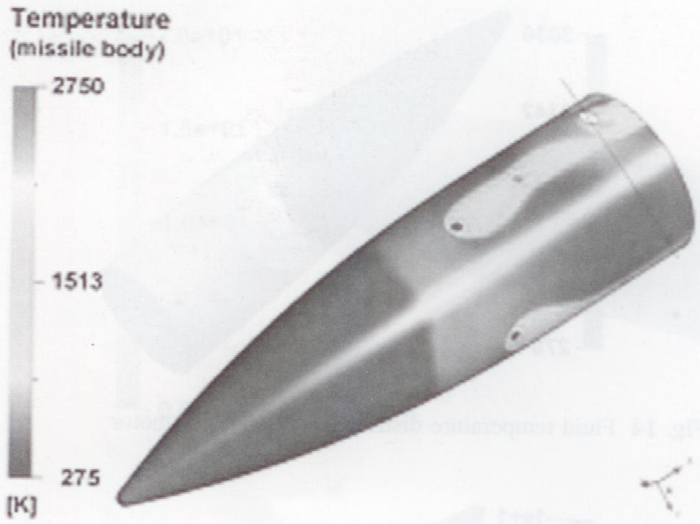

Fig. 8 Static temperature distribution on missile surface for case 1

Fig. 9 Heat flux distribution on the missile body

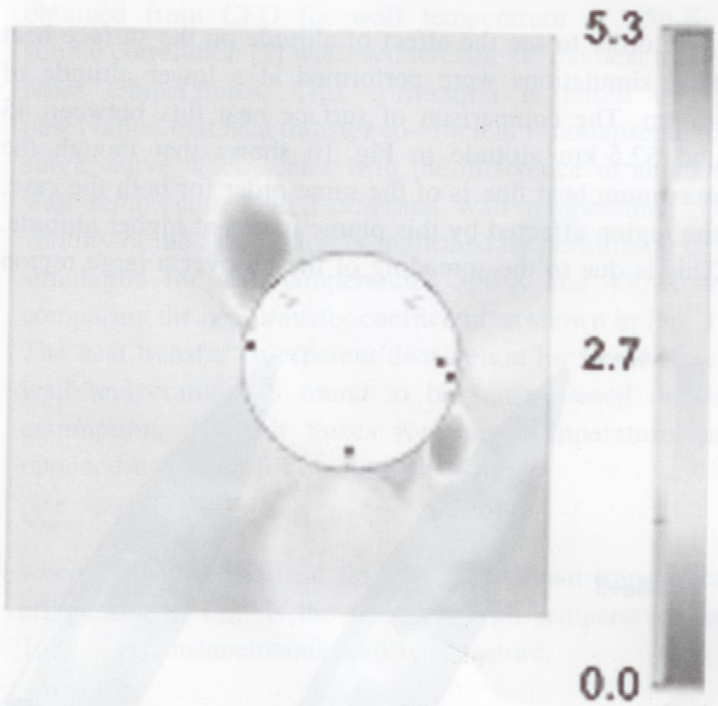

Fig. 10 Mach number contour in cross sectional plane passing through RCS motors for case 2

vernier jets can be seen from Fig. 4b. The zoomed view of velocity vector ahead of transverse jet is presented in Fig. 5. The low pressure suction region downstream of the

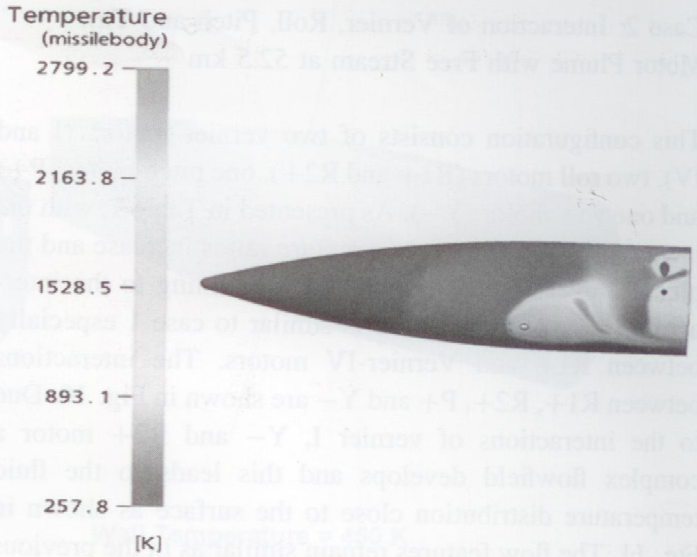

Fig. 11 Fluid temperature distribution for case 2

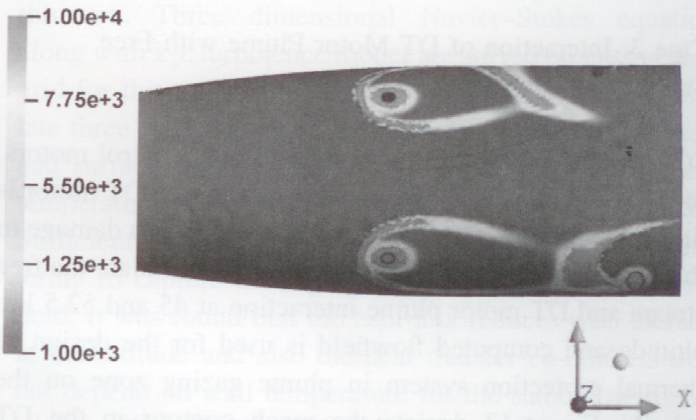

Fig. 12 Heat Flux distribution on the missile body for case 2

jet is seen from the static pressure plot in the plane passing through vernier motor in Fig. 6. It can be noticed from Figs. 4a and 6 that in the downstream of suction region due to vernier jet, there is sudden reduction in Mach number and increase in pressure which is due to a shock formed ahead of the roll motor plume. Velocity vector plot in Fig. 7 depicts the flow separation downstream of the shock and ahead of the roll motor jet. The gas temperature adjacent to the wall is plotted in Fig. 8. This shows that due to jet effect the average fluid temperature close to the wall is about 1,600 K, with a maximum temperature of about 2,750 K reaching around the periphery of the motors and at the shock location ahead of the jets. The heat flux distribution on the missile surface obtained for the isothermal wall temperature of 450 K is shown in Fig. 9. The negative values of heat flux indicate heat flow from fluid to the surface. The maximum heat flux ($\sim$1 w/cm^2) is found around the periphery of the motors and follows the surface temperature distribution pattern. This heat flux data is used to estimate the skin temperature.

Case 2: Interaction of Vernier, Roll, Pitch and Yaw Motor Plume with Free Stream at 52.5 km

This configuration consists of two vernier motors (I and IV), two roll motors (R1+ and R2+), one pitch motor (P+) and one yaw motor (Y−). As presented in Table 1, with the increase in the altitude, the pressure ratios increase and the plume bulges more. The flowfield pertaining to the interaction involved in this case is similar to case 1 especially between R1+ and Vernier-IV motors. The interactions between R1+, R2+, P+ and Y− are shown in Fig. 10. Due to the interactions of vernier I, Y− and R2+ motor a complex flowfield develops and this leads to the fluid temperature distribution close to the surface as shown in Fig. 11. The flow features remain similar as in the previous case. The surface heat flux distribution obtained for this configuration using the isothermal wall condition of 450 K is shown in Fig. 12.

Case 3: Interaction of DT Motor Plume with Free Stream at 45 and 52.5 km

DT motor is the largest among the attitude control motors. In the last phase of engagement scenario, only DT motor is fired for lateral displacement to cause maximum damage to the target. Simulations were carried out to simulate the free stream and DT motor plume interaction at 45 and 52.5 km altitude and computed flowfield is used for the design of thermal protection system in plume gazing zone on the missile. Figure 13 depicts the mach contour in the DT motor plane at 52.5 km altitude which shows the flow characteristics of a cross flow in supersonic stream. The fluid temperature distribution on the missile body in Fig. 14 shows the effect of shock and the plume expansion on the temperature distribution. The heat flux obtained for a wall temperature of 450 K is shown in Fig. 15. This shows a symmetric distribution of heat flux around the DT Motor and the maximum heat flux around the jet periphery.

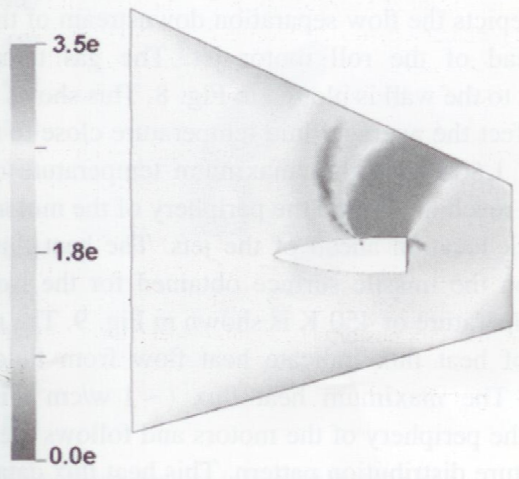

Fig. 13 Mach number contour in the DT motor plane

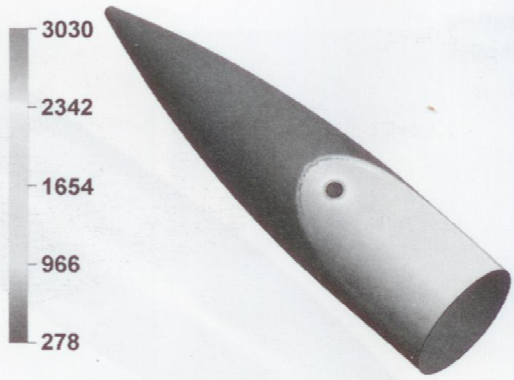

Fig. 14 Fluid temperature distribution around DT motor

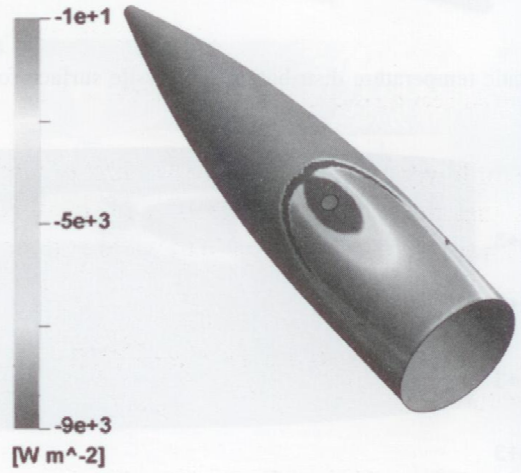

Fig. 15 Heat flux distribution around DT motor

In order to see the effect of altitude on the surface heat flux, simulations were performed at a lower altitude of 45 km. The comparison of surface heat flux between 45 and 52.5 km altitude in Fig. 16 shows that though the maximum heat flux is of the same order for both the case, the region affected by this plume is less at higher altitude. This is due to the spreading of the jet over a large region

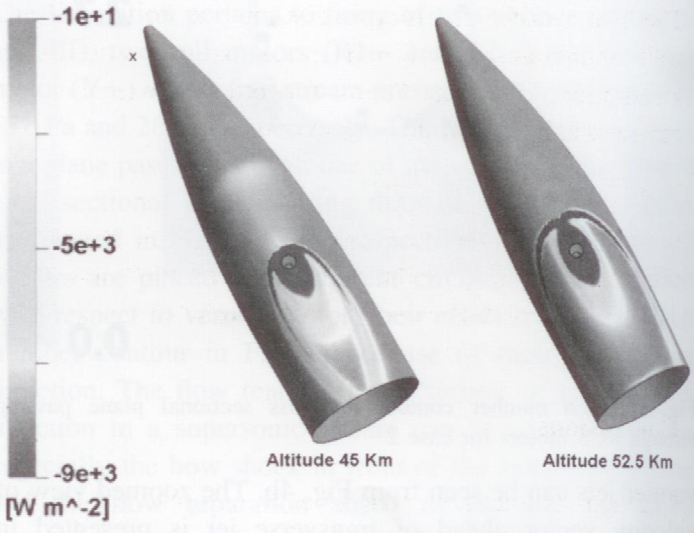

Fig. 16 Wall heat flux distribution for two altitudes

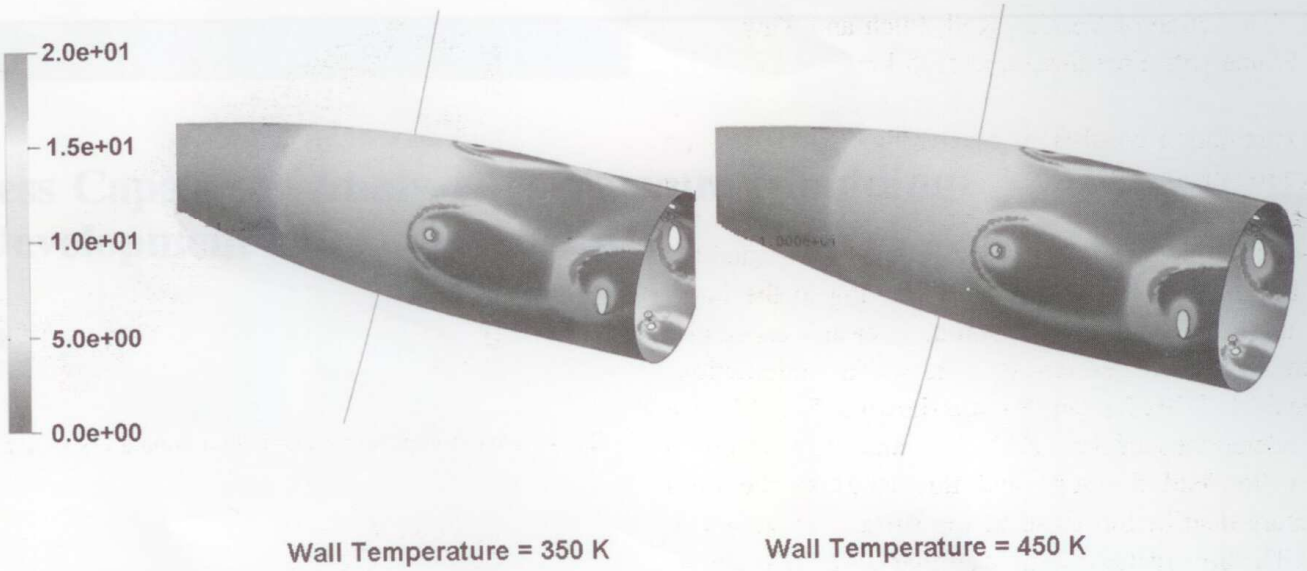

Fig. 17 Wall heat transfer coefficient for different wall temperatures

because of lower ambient pressure at a higher altitude. This ensures that the design capable of withstanding the heat load at lower altitude will be able to withstand the heat load at higher altitude also.

Estimation of Heat Flux for Different Wall Temperatures

In order to estimate the transient skin temperature rise, heat flux values at different wall temperatures were required. Using the adiabatic wall temperature and heat flux data obtained from CFD for wall temperature of 450 K, a simple correlation [7] was used to estimate the heat flux for other temperatures. This correlation is based on the observation that heat transfer co-efficient is collapsed into a single curve when scales with the difference of adiabatic wall temperature and isothermal wall temperature. The validity of the assumption is confirmed by performing CFD simulation for wall temperatures 350 K and 450 K and comparing the heat transfer coefficient as shown in Fig. 17. The heat transfer co-efficient distribution for two different wall temperatures is found to be same. Based on this assumption, the heat fluxes for other temperatures are obtained using the following expression.

$$Q_{new} = h \times (T_{aw} - T_{wall})$$

where 'Q_{new}' is the heat flux, 'h' is the heat transfer co-efficient and 'T_{aw}' is the adiabatic wall temperature and T_{wall} is the instantaneous wall temperature.

Conclusions

CFD simulations are carried out to compute the heat flux distribution on the missile surface caused due to the interaction of free stream with plumes of different control thrusters. Three dimensional Navier–Stokes equations along with k-ε turbulence model are solved on unstructured grid for this purpose. Three simulations are done to simulate three different sets of RCS firings at different altitudes and surface heat flux values obtained for isothermal wall temperatures 350, 450, 550 and 650 K for each case. Sufficient care is taken to provide appropriate grid clustering to capture the high gradients in the complex flowfield. It was found that the heat flux reduces with increase in the altitude and also the heat transfer co-efficient does not depend on wall temperature for the same flow configuration. The heat flux data obtained has been used for the prediction of surface temperature of the missile along its trajectory.

References

1. P. Champigny, R.G. Lacau, Lateral jet control for tactical missiles, AGARD Rep. **804**, 301–3057 (1994)
2. A. Ben-Yakar, M.G. Mungal, R.K. Hanson, Time evolution and mixing characteristics of hydrogen and ethylene transverse jets in supersonic crossflows. Phys. Fluids **18**(2), 026101 (2006)
3. L.A. Cassel, Applying jet interaction technology. J Spacecr. Rocket. **40**(4), 523–537 (2003)
4. G. Aswin, D. Chakraborty, Numerical simulation of transverse side jet with supersonic freestream. Aerosp. Sci. Technol. **14**, 295–301 (2010)
5. User Manual, CFX-10 (Ansys India Ltd., 2004)
6. User Manual, CFX Build 5.6 (AEA Software Ltd)
7. M.S.R. ChandraMurty, D. Chakraborty, Thermal response analysis of scramjet combustor walls to high speed turbulent reacting flows, in *Proceedings of SAROD-2009, Bangalore*, December 10–12, 2009, pp. 698–*710*